JOURNAL OF GEOPHYSICAL RESEARCH, VOL. 101, NO. A10, PAGES 21,501–21,513, OCTOBER 1, 1996

Ion acceleration at both the interior and exterior Alfvén waves associated with the magnetopause reconnection site: Signatures in cusp precipitation

M. Lockwood
Rutherford Appleton Laboratory, Chilton, Oxfordshire, England, United Kingdom

S. W. H. Cowley
Department of Physics and Astronomy, Leicester University, Leicester, England, United Kingdom

T. G. Onsager
Space Environment Center, National Oceanic and Atmospheric Administration, Boulder, Colorado

Abstract. We present evidence for the acceleration of magnetospheric ions by reflection off two Alfvén waves, launched by the reconnection site into the inflow regions on both sides of the reconnecting magnetopause. The "exterior" wave stands in the inflow from the magnetosheath and is the magnetopause, in the sense that the majority of the field rotation occurs there. The other, "interior" wave stands in the inflow region on the magnetospheric side of the boundary. The population reflected by the interior wave is the more highly energized of the two and appears at low altitudes on open field lines, immediately equatorward of the cusp precipitation. In addition, we identify the population of magnetosheath ions transmitted across the exterior Alfvén wave, as well as a population of magnetospheric ions which are accelerated, after transmission through the interior wave, by reflection off the exterior wave. The ion populations near the X line are modeled and, with allowance for time-of-flight effects, are also derived from observations in the dayside auroral ionosphere. Agreement between observed and theoretical spectra is very good and the theory also explains the observed total fluxes and average energies of the precipitations poleward of the open/closed field line boundary. The results offer a physical interpretation of all the various classifications of precipitation into the dayside ionosphere (central plasma sheet, dayside boundary plasma sheet, void, low-latitude boundary layer, cusp, and mantle) and allow the conditions in both the magnetosphere and the magnetosheath adjacent to the X line to be studied.

Introduction

Following the initial suggestion by *Petschek* [1964] of shocks standing in the inflow regions of a reconnecting current sheet, *Levy et al.* [1964] pointed out that reconnection at the dayside magnetopause will cause an initial tangential discontinuity boundary to decay into a series of MHD waves radiating from the reconnection site and which, in steady state, are often thought of as forming standing shocks in the inflow regions. Fast mode waves radiate isotropically from the reconnection site, but the group velocities of Alfvén waves (also called "intermediate mode" or "rotational discontinuity" and here abbreviated to RD) and slow mode waves are along and close, respectively, to the field-aligned direction. Because the Alfvén waves propagate at a higher speed, they form structures which lie closest to the magnetic separatrices, but the inflow toward the boundary causes them to lie inside the separatrices. Between these two rotational discontinuities (RDs) is the reconnection layer, also called the open low-latitude boundary layer (LLBL), containing structures associated with the slower slow mode waves between which would be any contact discontinuity where the inflows from the two sides meet. (However, the latter will not be significant for the collisionless plasmas at the magnetopause [*Lin and Lee*, 1993]). This structure of the reconnecting magnetopause has been discussed by *Heyn et al.* [1988] and *Cowley* [1995].

The major field rotation of the newly opened field lines, which thread the magnetopause, takes place at the two Alfvén waves that bound the reconnection layer. This has been demonstrated using analytic theory by *Heyn et al.* [1988] and using simulations by *Lin and Lee* [1993]. We here refer to these Alfvén waves as the exterior and interior RDs, on the magnetosheath and the magnetosphere boundaries of the LLBL, respectively, as shown in Figure 1a. The field is generally slightly higher on the magnetospheric side of the boundary, but the density is considerably lower (see,

Paper number 96JA01948.
0148-0227/96/96JA-01948$09.00

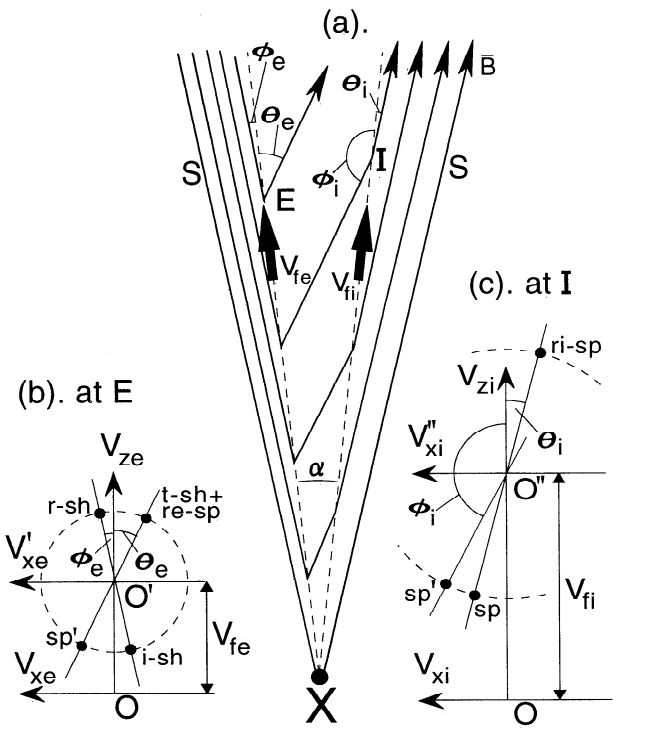

Figure 1. (a). Schematic illustration of a simplified magnetopause reconnection layer produced by a reconnection site labeled X. The dashed lines are the Alfvén waves which bound the reconnection layer (open low-latitude boundary layer) and lie inside the magnetic separatrices (S). The interior and the exterior waves stand in the inflow regions in the magnetosphere (to the right) and magnetosheath (to the left). The kinks in the newly open field lines ($\bar{B}$) at these rotational discontinuities (RDs) (labeled I and E, respectively) propagate away from the X line at speeds, V_{fi} and V_{fe}, where $V_{fi} > V_{fe}$. (b) The velocity space construction for point E, on the exterior RD, as used by *Cowley* [1982]. (c) The corresponding construction for point I on the interior RD. The plasma velocities along and normal to the interior RD are V_{zi} and V_{xi}, respectively; the corresponding velocities along and normal to the exterior RD are V_{ze} and V_{xe}. O is the origin in the Earth's frame, and O″ and O′ are the origins of the de Hoffman-Teller frames at I and E.

for example, the statistical studies by *Phan et al.* [1994]). Thus the Alfvén speed on the interior of the boundary V_{Asp} is usually higher than that on the exterior V_{Ash}. *Lin and Lee* [1994] have noted that the magnetosheath bulk flow is small near a dayside reconnection site and, as a result of this and the lower Alfvén speed, the field kink at the exterior edge (E in Figure 1a) moves away from the reconnection site at a speed V_{fe}, which is less than the speed V_{fi} with which the kink I moves along the interior edge of the LLBL. As shown in Figure 1a, the field inside the LLBL makes an angle ϕ_i with the interior RD and an angle θ_e with the exterior RD, and these are related by $\phi_i + \theta_e = \pi + \alpha$, where α is the angle between the two RDs. From this and the geometry shown in figure 1a, the angle θ_e is given by

$$\theta_e = \tan^{-1}\{\sin\alpha / [\cos\alpha - (V_{fe} / V_{fi})]\}. \quad (1)$$

Because the angle of the outflow wedge α is small (<5°) and $V_{fe} << V_{fi}$ the angle θ_e is small and ϕ_i is near π. This means that most of the field rotation takes place at the boundary between the magnetosheath and the LLBL and the exterior RD is a much stronger contributor to the total current sheet than the interior RD. Although the field rotation at I is small, the interior RD can sometimes be detected as a difference in the inclination of the field orientation in the LLBL, with respect to that in the magnetosphere [see, for example, *Hapgood and Bryant* [1992, Figure 6]. *Cowley et al.* [1983] have shown that this field inclination in the dayside LLBL is as predicted for the reconnection theory.

In this paper, we consider what happens to ion populations when they interact with current sheets at the magnetopause. As virtually all the field rotation (and thus the current) is at the two Alfvén waves, we neglect the effect of any waves and structures within the reconnection layer between them. *Cowley* [1982] noted that there were three populations incident on the magnetopause: the sheath population from the outside and the ionospheric and ring current populations from the inside. Each of these populations will interact with the current sheet and some ions will be reflected by the boundary and some will be transmitted across it. Cowley assumed that in either case, the pitch angle of the ions was conserved on interaction with the current sheet. This is clearly not a good assumption when dealing with individual particles, but when dealing with a statistical ensemble, the scattering which may be present does not greatly alter the form of the distribution function. He predicted D-shaped distribution functions (truncated, drifting Maxwellians) of the transmitted and reflected populations. Almost 10 years after these predictions were made, they were verified in observations of accelerated flows at the dayside magnetopause [*Gosling et al.*, 1990a; b; *Smith and Rodgers*, 1991; *Fuselier et al.*, 1991]. In addition to showing the D-shaped distribution functions of the accelerated injected ion flows in the open LLBL, Smith and Rodgers applied the stress-balance test and showed that the cutoff was close to the field line velocity, as also predicted by the theory. In addition, Fuselier et al. studied He^+ and He^{++} ions because these are mainly of magnetospheric and magnetosheath origin, respectively. They found not only the injected sheath ions, but also all populations (incident, transmitted, and reflected) were as predicted by *Cowley* [1982], on both sides of the boundary.

These predictions by *Cowley* [1982] only considered the effect of particles interacting with a single RD on the outside of the open LLBL. We here identify this magnetopause with the dominant (exterior) Alfvén wave emanating from the reconnection site and standing in the magnetosheath inflow. In this paper, we extend the predictions of Cowley to also consider the interaction of the particles with the weaker (interior) Alfvén wave launched from the diffusion region into the magnetospheric inflow region. It is shown that this second interaction generates a more energized population of magnetospheric ions on the most recently opened field lines. We identify such a population in data from a low-altitude satellite. To do this, we must first allow for the velocity filter effect caused by the dependence on energy of the ions' flight times from the magnetopause to the ionosphere. This population is likely to have been classified as LLBL or even dayside boundary plasma sheet (BPS) in the past because of the high fluxes of ions at high energies. These high-energy fluxes are much higher than expected from the magnetosheath, even allowing for the current sheet acceleration

Table 1. Major Ion Populations at the Magnetopause

Label*	Origin	Present Location	History
i-sh	magnetosheath	magnetosheath	yet to encounter exterior RD
sp	magnetosphere	magnetosphere	yet to encounter interior RD
r-sh	magnetosheath, i-sh	magnetosheath	reflected off exterior RD
t-sh	magnetosheath, i-sh	LLBL	transmitted through exterior RD
t-sh	magnetosheath, i-sh	magnetosphere	transmitted through both RDs
sp′	magnetosphere, sp	LLBL	transmitted through interior RD
ri-sp	magnetosphere, sp	magnetosphere	reflected off interior RD
re-sp	LLBL, sp′	LLBL	reflected off exterior RD
re-sp	LLBL, sp′	magnetosphere	reflected off exterior RD and then transmitted through interior RD
t-sp	LLBL , sp′	magnetosheath	transmitted through exterior RD

RD is rotational discontinuity; LLBL is low-latitude boundary layer.

* The i, r, and t refer to populations incident on, reflected off or transmitted through, respectively, an RD. The e and i (following r) denote the exterior and interior RD, respectively. The sh and sp are magnetosheath and magnetosphere, respectively.

described by *Cowley* [1982]. We here show that these ions are energized by reflection off the interior Alfvén wave and are on the most recently opened field lines, as is also indicated by the electron precipitation data.

Theory

In this paper, we will consider the cusp pass by the Defense Meteorological Satellite Program (DMSP) F7 satellite on January 26, 1984, which has previously been presented by *Newell et al.* [1991a], modeled by *Onsager et al.* [1993] and *Alem and Delcourt* [1995], and studied by *Lockwood et al.* [1994]. Lockwood et al. deduced that the Alfvén speed in the magnetosheath at the X line was V_{Ash} = 190 km s^{-1} for this case. We here consider an interior Alfvén speed of V_{Asp} = 600 km s^{-1} on the magnetospheric side of the X line. The choice of this and other values for input model parameters will be discussed in the following sections. These two Alfvén speeds control the speed with which points E and I evolve away from the reconnection site in Figure 1a. The theory of an ideal MHD rotational discontinuity by *Hudson* [1970] predicts that plasma will flow through the RD at the local Alfvén speed in the de Hoffman-Teller (dHT) frame in which the electric field is zero [*de Hoffmann and Teller*, 1950]. As discussed by *Cowley and Owen* [1989] and *Lockwood* [1995], this means that the point E will move at speed V_{fe} in the Earth's frame such that $V_{fe} + V_{sh} \cos\phi_e = V_{Ash}$ where ϕ_e is the angle that the sheath field makes with the RD, as shown in Figure 1b and V_{sh} is the component of the (boundary tangential) sheath flow along the projection of the sheath field onto the RD. Similarly, in general, the point I moves at V_{fi} in the Earth's frame such that $V_{fi} + V_{sp} \cos\theta_i = V_{Asp}$, where V_{sp} is the field-aligned component of the flow inside the magnetosphere and θ_i is defined in Figure 1a. At the X line, $\cos\theta_i = \cos\phi_e = 1$, to a very good approximation. Because of the small value of the field-aligned sheath flow at the X line deduced by *Lockwood et al.* [1994] (V_{sh} = -22 km s^{-1}), point E in Figure 1a moves along the exterior LLBL boundary at V_{fe} = 168 km s^{-1} , which is close to V_{Ash}. Figure 1c is constructed for a general V_{sp}; however, this magnetospheric flow is likely to be close to zero and point I will then move along the interior edge of the open LLBL at $V_{fi} = V_{Asp}$.

At this point, we wish to explain the nomenclature that we have adopted to name ion populations because this will be used extensively throughout the paper. The general form of the classification is ab-c, where c gives the origin if the ions (and is either sp or sh for the magnetospheric and magnetosheath ion populations, respectively): a may be i, t, or r, denoting populations incident on, transmitted through, or reflected off, respectively, an Alfvén wave which, where necessary, is identified by b (either e for the exterior wave or i for the interior wave). Thus, for example, ri-sp is the population of magnetospheric ions which have been reflected off the interior wave, t-sh is the population of magnetosheath origin which is transmitted through one or both of the waves. The full list of populations considered is given in Table 1.

Figure 1b shows the velocity space construction used by *Cowley* [1982] to predict the particle distributions (t-sh and r-sh) produced from the incident sheath population (i-sh) by transmission through and reflection off, respectively, the exterior RD at points like E. In addition, the population within the LLBL of magnetospheric origin (sp′) is transmitted through and reflected off the magnetopause to produce populations called t-sp and r-sp, respectively. The velocity V_{ze} is along the exterior RD at E and V_{xe} is along the outward normal to that RD: the V_{ze},V_{xe} frame, with origin O, is at rest relative to the Earth while the V'_{ze},V'_{xe} frame, with origin O′, is the local dHT frame at E. The magnetosheath and LLBL fields make angles θ_e and ϕ_e with the RD at E. The points in Figure 1b, lying on the dashed circle of radius V_{Ash} and centered at O′, show the velocities of the peak phase space density of the populations. This form of the construction is used and explained in greater detail by *Lockwood* [1995]. *Cowley's* [1982] theory has been shown to be very successful in predicting the distribution functions on both sides of the magnetopause [*Gosling et al.*, 1990a; b; *Fuselier et al.*, 1991; *Smith and Rodgers*, 1991]. We here extend the predictions to show that there will be two components of the r-sp ions. One is produced by reflection off the interior RD and is here termed ri-sp; the other (re-sp) is transmitted through the interior RD (with negligible acceleration because the field rotation at I is small; that is, $\theta_i + \phi_i \approx \pi$, so that the popula-

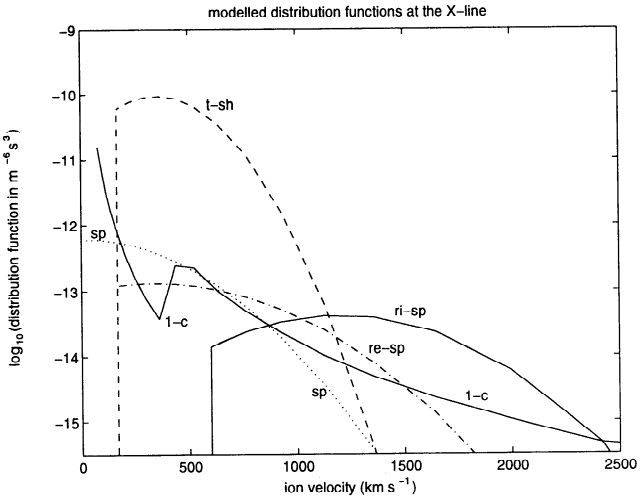

Figure 2. Modeled field-parallel segments of the distribution function of magnetospheric ion populations. Here t-sh is the transmitted magnetosheath population (dashed line); sp is the magnetospheric population on closed field lines (dotted line), which gives the re-sp population (dot-dashed line) when reflected off the exterior RD and ri-sp (solid line) when reflected off the interior RD. (see Table 1 for population descriptions.) The t-sh population has a density and temperature of 1.2×10^7 m^{-3} and 4.9×10^6 K, respectively; the sp population has density 4.3×10^5 m^{-3} and temperature 1.5×10^7 K, with all values relating to the field-parallel direction. The Alfvén speed on the magnetospheric side of the boundary is 600 km s^{-1} and on the magnetosheath side of the boundary it is 190 km s^{-1}, where the field-aligned sheath velocity is -22 km s^{-1}. The density reflection factors for the sp population at the exterior and interior RDs are $r_e = 0.4$ and $r_i = 0.1$ respectively, and the corresponding field-parallel heating factors are $h_e = 1.5$ and $h_i = 1.3$. The solid line labeled 1-c is the one-count level of the ion detector on the DMSP F7 satellite.

tion sp′ in Figure 1 is almost identical to sp), subsequently being accelerated by reflection at the exterior RD (at E). (See Table 1 for a summary of the various populations and their origins and histories). It should be noted that there will be additional ion populations present which are formed by multiple reflections off the two RDs. These are not considered further in this paper because the small reflection coefficients will result in such populations adding only very small flux contributions to regions of velocity space dominated by the populations listed in Table 1.

The velocity space construction for the interior RD at I is shown in Figure 1c, where the local dHT frame V''_{zi}, V''_{xi} has an origin at O″. Because the angles θ_e and θ_i are small enough to make $\cos\theta_e = \cos\theta_i = 1$ a valid approximation near the X line, the peak phase space density of the re-sp population appears at $(V_{Ash} + V_{fe})$ and that of the ri-sp population at $V_{Asp} + V_{fi} = 2V_{Asp}$. The temperature of the populations means that there is a spread of ion velocities about the peak phase space density in each case. Ions of the sp population moving away from the RD at a speed greater than the field line speed in the Earth's frame will not encounter it, and so the ri-sp and re-sp populations are truncated at minimum velocities of V_{fi} and V_{fe}, respectively. Because $V_{Asp} > V_{Ash}$ and $V_{fi} > V_{fe}$, the population reflected off the interior RD, ri-sp, is considerably more accelerated than those populations reflected off and transmitted through the exterior RD (re-sp and t-sh, respectively).

Using the theory of *Cowley* [1982], it is possible to predict the distribution functions $f(v)$ of all the populations. An example of a set of field-aligned ion populations in the magnetosphere is given in Figure 2. These are modeled using the inputs listed in Table 2, which will be derived from fits to satellite data and discussed in subsequent sections. The dashed line in Figure 2 is the transmitted sheath population, t-sh, and is that deduced by *Lockwood et al.* [1994] from the same low-altitude satellite data as is studied here. The dotted line in Figure 2 is the magnetospheric population sp on closed field lines, which here is given a concentration $N_{sp} = 4.3\times10^5$ m^{-3} and a temperature T_{sp} of 1.5×10^7 K and is isotropic. The effect of an anisotropic form of the sp distribution function is discussed in the appendix. The solid line in

Table 2. Model Inputs Used in Figures 2 and 7.

Symbol	Meaning	Value
V_{Asp}, km s^{-1}	Alfvén speed at interior RD	600
V_{sp}, km s^{-1}	field-aligned bulk flow of sp ions	0
V_{fi}, km s^{-1}	dHT velocity at interior RD	600
V_{Ash}, km s^{-1}	Alfvén speed at exterior RD	190
V_{sp}, km s^{-1}	field-aligned bulk flow of i-sh ions	-22
V_{fe}, km s^{-1}	dHT velocity at exterior RD	168
N_{sp}, m^{-3}	concentration of field-aligned sp population	4.3×10^5
T_{sp}, K	field-aligned temperature of sp population	1.5×10^7
N_{tsh}, m^{-3}	concentration of field-aligned t-sh population	1.2×10^7
T_{tsh}, K	field-aligned temperature of t-sh population	4.9×10^6
r_i	fraction of sp ions reflected off interior RD	0.1
h_i	heating factor of sp ions on reflection off interior RD	1.3
r_e	fraction of sp′ ions reflected off exterior RD	0.4
h_e	heating factor of sp′ ions on reflection off exterior RD	1.5

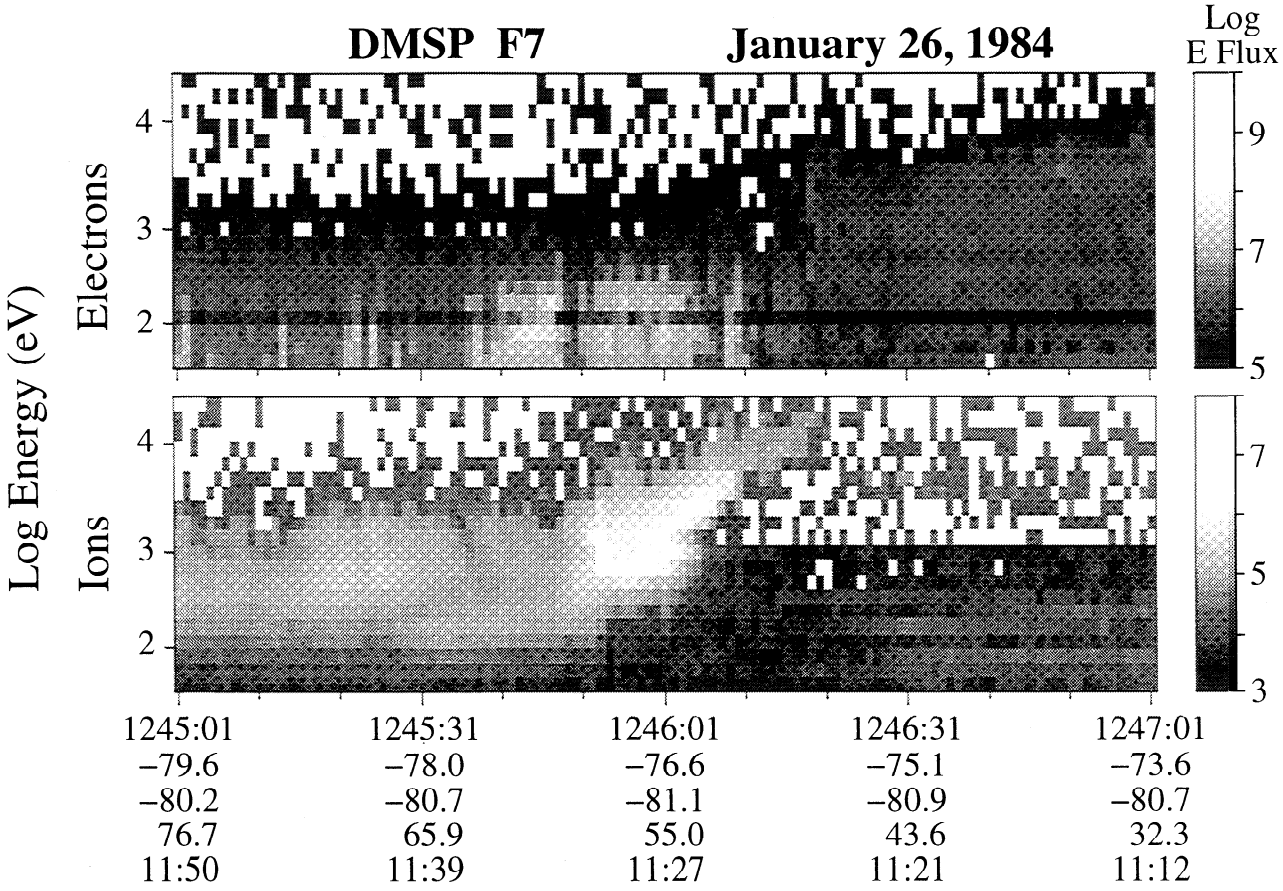

Figure 3. (top) Electrons and (bottom) ions observed by the DMSP F7 satellite during a cusp crossing on January 26, 1984. Differential energy flux is logarithmically gray-scaled as a function of observing time and the logarithm of energy. The precipitation classed as "cusp" by *Newell et al.* [1991a] is seen between 1245:53 and 1246:09. This paper is primarily concerned with the population of high-energy ions seen immediately equatorward of the cusp between 1246:09 and 1246:20.

Figure 2 is that part of the sp population which has been reflected off the interior RD (ri-sp), and the fraction of the sp population reflected is taken to be $r_i = N_{\text{ri-sp}}/N_{\text{sp}} = 0.1$. *Lockwood et al.* [1994] found some evidence that there was some weak heating on interaction with the RD, and this is allowed for here by raising the temperature of the ri-sp population by a factor of $h_i = 1.3$ over T_{sp}. The dot-dashed line in Figure 2 is that part of the sp population which has been reflected off the exterior RD (re-sp), and the fraction of the sp population reflected is taken to be $r_e = 0.4$ with a heating factor of $h_e = 1.5$.

Figure 2 gives the field-parallel distribution functions $f(v)$ for populations of ions generated in the immediate vicinity of the X line. They are dominated by the t-sh population at low ion velocities v and by the ri-sp population at high velocities with the phase space density f for these two becoming equal at v near 1100 km s^{-1}. We wish to identify these populations in low-altitude satellite data. To do this, we make use of the fact that such ions from the immediate vicinity of the X line will have the longest flight time of all the ions which are injected and/or accelerated by the reconnection process and which are seen at any one point in the ionosphere and thus at one observation time t_s, therefore they have the lowest velocity (here called the cut-off velocity, v_{ic}) at that t_s [*Lockwood and Smith*, 1992; *Lockwood*, 1995]. For adiabatic, scatter-free motion between the magnetopause and the ionosphere, they will be seen with the same velocity v_{ic} as at the magnetopause, and by Louiville's theorem, they will also have the same phase space density $f(v_{ic})$. We here adopt the procedure of *Lockwood et al.* [1994] to identify the phase space density at the low-velocity cutoff $f(v_{ic})$ at different observation times t_s and thus reconstruct the distribution function $f(v)$ in the immediate vicinity of the X line.

DMSP F7 Data From January 26, 1984

Figure 3 shows the electron (top) and ion (bottom) data from the DMSP F7 satellite pass through the cusp near 1246 UT on January 26, 1984, first published by *Newell et al.* [1991a] who classified the precipitation as "mantle" up to 1245:53 and as cusp in the interval 1245:53-1246:09. The differential energy flux is logarithmically shaded and plotted as a function of observing time and the logarithm of energy. The satellite can be seen to fly equatorward through a quasi-steady mantle/cusp dispersion plume. *Onsager et al.* [1993] have used the theory by *Cowley* [1982], as discussed above, in a steady state model of the injection, acceleration, and precipitation of solar wind plasma on newly opened field

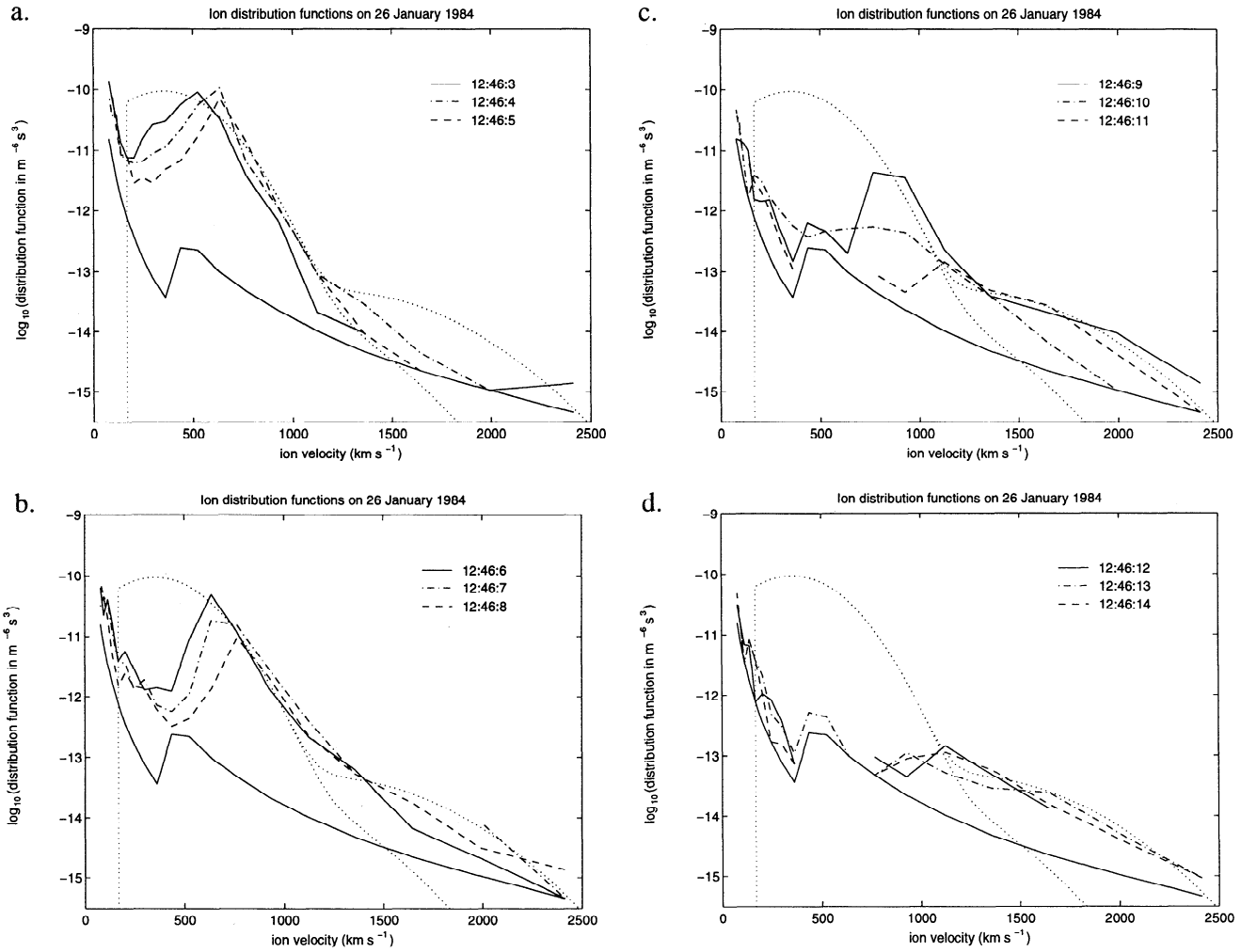

Figure 4. Ion velocity distribution functions $f(v)$ for various times in the pass shown in figure 3 labeled by the observation time t_s at the end of each 1-s instrument cycle: (a) 1246:3- 1246:5, (b) 1246:6-1246:8, (c) 1246:9-1246:11, (d) 1246:12-1246:14, (e) 1246:15-1246:17, (f) 1246:18-1246:20 UT. Bottom solid lines are the one-count level of the instrument, the top dotted lines are the sum of the t-sh and ri-sp populations in Figure 2 (which will be the dominant pair of populations when the ri-sp ions are present), and the bottom dotted lines are the sum of t-sh and re-sp (which will dominate when ri-sp ions are absent).

lines. They successfully reproduced the major features of Figure 3. However, one feature not well reproduced by the Onsager et al. model concerns the ion data seen just after 1246:10 UT, immediately equatorward of the cusp region. Figure 3 shows that the ion dispersion ramp was continuous across the equatorward edge of the cusp and continued with decreasing latitude such that detectable fluxes were seen up to 20 keV. Onsager et al. did not find such high ion energies; instead, their model produced a plateau with roughly constant peak energy of detectable ion flux at about 7 keV. The same feature was the subject of a paper by *Alem and Delcourt* [1995] who attempted to simulate it by using non-adiabatic magnetospheric ion trajectories in a closed field-line magnetic cusp topology.

The fact that these energetic ions immediately equatorward of the cusp show a dispersion ramp that is continuous with the cusp ions strongly suggests that their acceleration and transport mechanisms are intimately linked with those of the cusp ions. As pointed out by *Alem and Delcourt* [1995], this is not explained by their non-adiabatic trajectory theory. In addition, the electron data appear to place these ions on newly opened field lines, like the cusp. Close to the equatorward edge of these ions at 1246:20 UT, there is a step-like change in the electron data (most easily seen at energies between 500 eV and 5 keV). Equatorward of this change, the electrons are magnetosphere-like and the step is consistent with the loss of field-parallel energetic electrons along newly opened field lines [*Gosling et al.*, 1990b]. Immediately poleward of this "electron edge," the electron spectrum is typical, in shape and energies, of the magnetosheath; however, fluxes are lower. This is consistent with the maintenance of quasi-neutrality in the cusp/LLBL region [*Burch*, 1985] because ion fluxes here are also low. At the cusp boundary, the flux of magnetosheath electrons rises with increasing latitude, in concert with the rise in ion fluxes.

Figure 4 shows the sequence of field-parallel ion distribution functions $f(v)$ seen at 1246:03-1246:20, during which the satellite crossed the equatorward edge of the cusp and moved to the electron edge. Figures 4a-4f each show three consecutive observed $f(v)$, with the lower solid line giving the

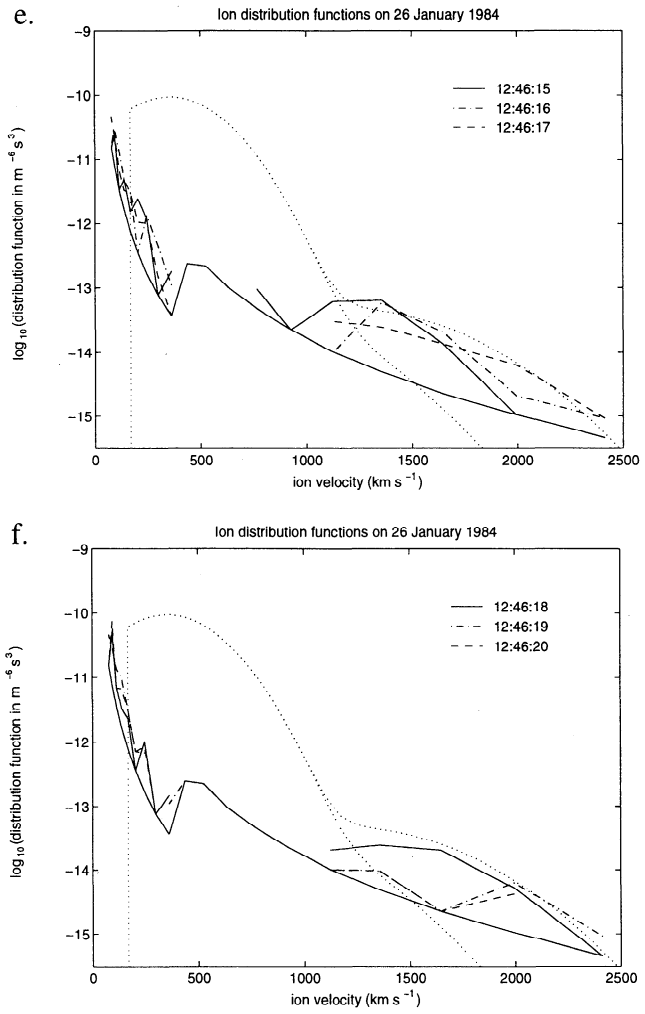

Figure 4. (continued)

instrument one-count level. In addition, Figures 4a - 4f each show the same pair of dotted lines, which are combinations of the modeled plasma components shown in Figure 2; one is the sum of the t-sh and ri-sp populations, the other is the sum of the t-sh and re-sp populations. These two lines differ at high v because fluxes are higher there for the ri-sp ions than for the re-sp. We show these two dotted lines because, as discussed later, we expect the ri-sp population to be present on any one newly opened field line for a limited time only; when present, the ri-sp population will dominate at high v. However, when the ri-sp ions are either absent or of greatly reduced flux, the re-sp population may be revealed. Figures 4a and 4b are for times when the satellite was still in the cusp region and show the low-velocity cutoff of $f(v)$ discussed by *Lockwood et al.* [1994]; this cutoff can be seen to move to higher v (that is, v_{ic} increases) at later times and $f(v_{ic})$ remains close to the two dotted lines (which are virtually identical at these lower v, where the t-sh population dominates). This is in agreement with the predictions, due to the fact that Figure 2 was constructed using the t-sh population deduced from these data by *Lockwood et al.* [1994]. In Figure 4c, the satellite reaches the equatorward edge of the cusp at 1246:09, after which (Figures 4d-4f) the cutoff generally continues to progress along the top dotted line. This is consistent with the ri-sp population becoming the dominant contribution to the ion flux at high v in the vicinity of the X line, as is predicted by Figure 2.

Lockwood et al. [1994, 1995] noted that both v_{ic} and $f(v_{ic})$ were difficult to define accurately from the distribution function $f(v)$ measured at each observation time t_s. Instead, they studied the time series of phase space density $f(t_s)$ for each energy channel, i.e., at constant ion velocity, v. As a satellite moves toward the open/closed boundary, the cutoff velocity v_{ic} will rise above that of a given channel of the detector. As this happens, there will be a decrease in $f(t_s)$ for that channel. The accuracy of the technique of using this decrease to define v_{ic} and $f(v_{ic})$ has been verified using simulated data by *Lockwood and Davis* [1996]. *Lockwood et al.* [1994, 1995] used the technique to define the $f(v)$ of the t-sh population that came from the immediate vicinity of the X line. We here extend the method of Lockwood et al. to higher energies to study the ri-sp population that came from near the X line. Figure 5 shows the sequences of $f(t_s)$ observed in each channel (here labelled by the energy $E = mv^2/2$). Figure 5b shows those for energies at which the t-sh population dominates, whereas Figure 5a also shows the higher energies for which Figure 2 predicts the ri-sp population will dominate. In all channels, a decay in $f(t_s)$ can be seen. After the decay, the phase space density is mostly constant at the one-count level for that channel. For each channel, the onset of the main decay in $f(t_s)$ has been marked in Figures 5a and 5b (circles). These values are again plotted in Figure 6 (circles). Because each of these points is close to the cutoff, this is a composite plot of the dominant ion populations close to the X line. In addition, any clear cutoff values from the $f(v)$ plots in Figure 4 are added (Figure 6, crosses). The plot shows two clear populations, consistent with the behavior seen in Figure 4, where the cutoff values remained close to the dotted line, which is the sum of modeled t-sh and ri-sp populations. Both are fitted here with drifting Maxwellian distributions. The population dominant at v below 1100 km gave the lower temperature ($T = 4.91\times10^6$ K), higher concentration ($N = 1.20\times10^7$ m^{-3}), and lower bulk field-aligned drift ($V = 355$ km s^{-1}) values listed in Figure 6 (bottom left). The population that is dominant above $v = 1100$ km is fitted with the higher temperature ($T = 2.00\times10^7$ K), lower concentration ($N = 4.33\times10^4$ m^{-3}), and higher drift ($V = 1180$ km s^{-1}) values also given in Figure 6 (top right).

Interpretation

Given the theoretical predictions presented in Figure 2, we here associate the two fitted populations in Figure 6 with the t-sh and ri-sp populations predicted for the structure of the open LLBL shown in Figure 1a. The t-sh population is as discussed by *Lockwood et al.* [1994], who used it to make deductions about the magnetosheath conditions near the reconnection site. We here concentrate on the implications of the fitted ri-sp population. The fitted velocity of peak phase space density is $2V_{fi} = 1180$ km s^{-1}, giving $V_{Asp} \approx 600$ km s^{-1}.

The data from just equatorward of the higher energy ions (at around 1246:31) are used to define the field-aligned sp population. The concentration ($N_{sp} = 4.3\times10^5$ m^{-3}) and temperature ($T_{sp} = 1.5\times10^7$ K) adopted here are as used to generate Figure 2 and give an $f(v)$ which just rises above the one-count level at $v \approx 700$ km ($E = 2.55$ keV), where an

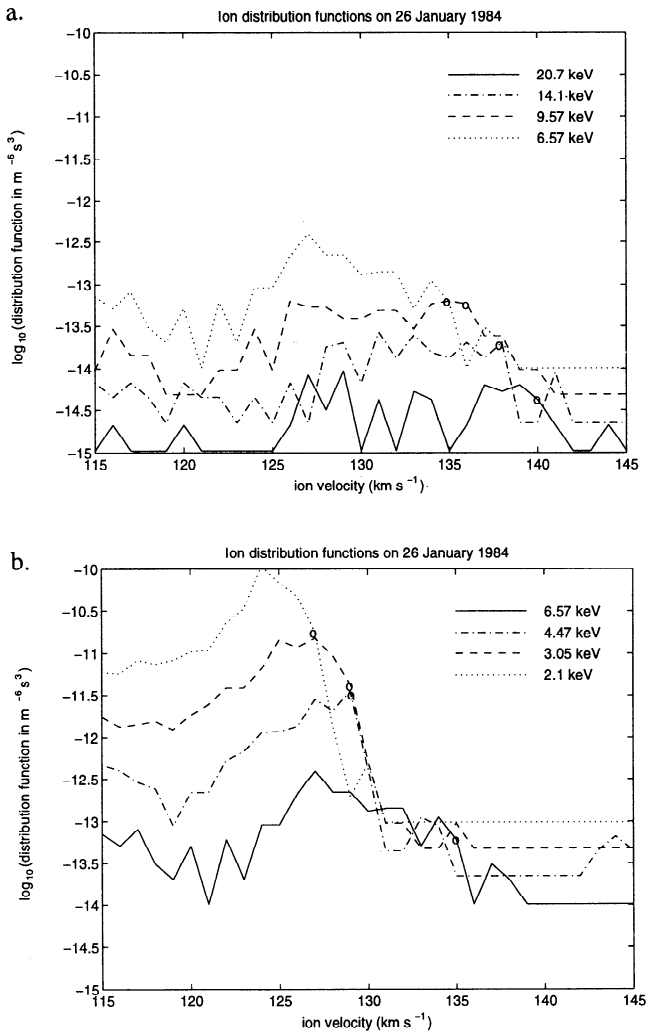

Figure 5. Time series of ion phase space density $f(t_s)$ for various energy channels, $E = mv^2/2$, (a) 6.57 - 20.7 keV and (b) 2.10-6.57 keV, for the pass shown in Figures 3 and 4. Time $t_s = 0$ is here defined to be 1244:00 UT. Circles show our best estimates of the low-velocity cutoffs $f(v_{ic})$ at the start of the decay as the satellite emerges through the equatorward boundary of the cusp.

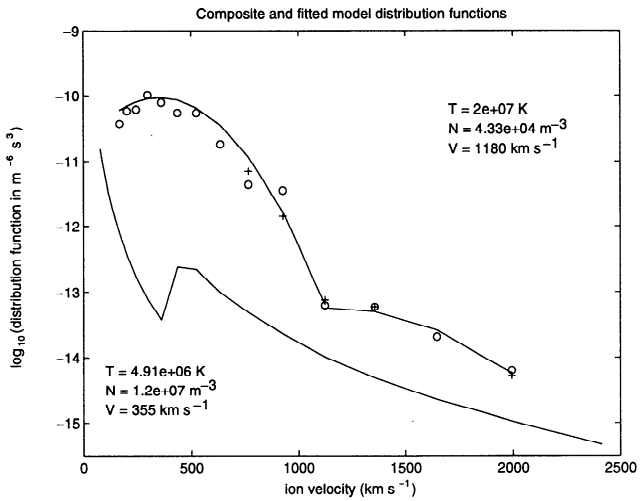

Figure 6. The field-aligned ion distribution function of particles from the reconnection site. The circles are $f(v_{ic})$ where the cutoff is defined from the $f(t_s)$ plots (Figure 5), whereas crosses are those from the $f(v)$ plots (Figure 4). The one-count level is shown as in Figures 2 and 4. These ions at the low energy/velocity cutoff have the longest flight time and were thus the first to be injected; therefore they originated from the reconnection site. Two drifting Maxwellian populations have been fitted to the data from above and below (and both including) the E = 6.57 keV channel (corresponding to an ion velocity $v \approx 1100$ km s^{-1}). The fitted density N, temperature T, and velocity of peak phase space density, V, are given in both cases, with the population dominant at v below 1100 km s^{-1} at bottom left and that dominant above v = 1100 km s^{-1} at top right.

isolated patch of single counts was indeed detected (see Figure 3). However, most of the sp population remains hidden below the one-count level, and thus these values are uncertain. The r_i factor required is then $(N/N_{sp}) = 0.1$ and the h_i factor is $(T/T_{sp}) = 1.3$, yielding the above derived values of the concentration and temperature for the ri-sp population seen at v ≥ 1100 km s^{-1}. These were the values adopted when generating Figure 2. For this pass, the magnetospheric sp population is of such a low concentration that it is largely hidden, being below the one-count level at most velocities. Using simulated spectra, like those in Figure 2, we find that N_{sp} could be varied by no more than about 20% before detectable changes in the count rate would be seen at $v > 500$ km s^{-1}. On this basis, the uncertainty of the reflection coefficient r_i is roughly ±0.02. The temperature T_{sp} adopted appears to be somewhat lower than is typically found near the magnetopause. However, the low count rates mean that values up to twice as large could be used to fit the spectra. A unity heating factor (h_i = 1) and a temperature T_{sp} of 2 × 10^7 K would be equally consistent with the data. Thus the heating factor is poorly defined. However, at this point, we must also note that the sp population seen by DMSP F7 is within the loss cone and thus will have a lower concentration (and could have a lower temperature) than at larger pitch angles, outside the loss cone. The Alfvén wave will reflect magnetospheric ions of all pitch angles, and the larger pitch angle ions will be scattered such that the ri-sp and re-sp populations will not show a loss cone. These anisotropy effects mean that the reflection and heating factors quoted here, which are derived from the field-parallel parts of all ion populations only, will not be good estimates of the values that consider ions of all pitch angles. This point is addressed further in the appendix.

Figure 2 gives the populations of ions generated in the immediate vicinity of the X line only (i.e., immediately after the field line is reconnected). Similar constructions can be made to predict the populations produced at other locations (and subsequent times) as the field line evolves away from the X line. In general, the precipitation seen at low altitudes will be a convolution of these changing source populations with time-of-flight effects, as recently modeled for the t-sh population by *Lockwood* [1995]. However, a less complicated model of the precipitation very close to the open/closed separatrix can be made with one simplifying assumption, namely, that the populations produced at the two Alfvén

waves (t-sh, ri-sp, and re-sp) do not depend on position relative to the X line. In reality, the populations will change because the field line accelerates and the sp ions are lost as they either escape across the both magnetopause RDs (giving rise to the t-sp population) or are reflected by them (to give the ri-sp and re-sp populations). In addition, the t-sh population will also vary with position because of the spatial structure of the magnetosheath, and the ri-sp population will vary because the interior RD accelerates (raising the energy of any reflected ions, but probably causing the field line kink at I to straighten and reducing the reflection coefficient r_i). Because of the velocity filter effect, each ion velocity observed at any one time t_s has a unique source location on the magnetopause, and thus the spectrum will, in general, be somewhat distorted by spatial gradients in the magnetopause characteristics. The appendix provides a discussion of why the loss of sp ions can be neglected. Because we are concerned only with features relatively close to the open/closed boundary, this assumption allows us to neglect the effect of changing source populations and considerably simplify the discussion.

This approach makes allowance for time-of-flight effects straightforward. It is possible to predict the population seen by a low-altitude satellite by simply truncating the t-sh, re-sp, and ri-sp spectra shown in Figure 2 at the time-of-flight cutoff velocity v_{ic}. This is because ions with velocity less than v_{ic} have not had sufficient time to reach the satellite, but ions with velocity greater than v_{ic} have the same phase space density as at the (uniform) source. In addition, all the magnetospheric population, sp, will be present at velocities below v_{ic}, but sp ions with $v > v_{ic}$ will have either escaped through the magnetopause RDs or will have been reflected off them. If the satellite, at a time t_s , observes a field line which was reconnected at a time t_o , the time elapsed since reconnection is t_s - t_o and the lowest velocity (longest flight time) ions that can be seen will have a cutoff velocity of v_{ic} = $d/(t_s - t_o)$, where d is the distance along the field line from the X line to the altitude of the satellite. Thus, for an assumed distance d, those parts of spectra t-sh, ri-sp, and re-sp which have reached the satellite are known as a function of t_s - t_o , as is the part of the sp population which remains. The integral fluxes of each population in the energy range of the DMSP F7 ion detector (30 eV-30 keV) can then be calculated for each t_s - t_o , the sum of which gives the total integral flux. Integral flux F is related to phase space density f and differential number flux J by $F = \int J\, dE = \int f\, (2E/m^2)\, dE$, where E is energy and m is the ion mass. Figure 7 shows the results for an assumed value of $d = 20\ R_E$ (Earth radii) for the populations shown in Figure 2. The choice for d is not important, as it only influences the scale of the t_s - t_o axis and does not alter the form nor the magnitude of the flux variations. Thus, for example, a d of $10R_E$ would produce a Figure identical to Figure 7, except that the t_s - t_o axis scale would be halved. Figure 7 (top) shows the modeled total flux as a dot-dashed line, whereas Figure 7 (middle) shows the integral fluxes of each of the modeled populations using the same linetypes and labels as Figure 2 and as listed in Table 1. Note that the left hand edge of Figure 7 at t_s -t_o = 0 is the open/closed field line boundary and that t_s - t_o > 0 is open field lines. The dot-dashed line in Figure 7 (bottom) shows the modeled variation of the average ion energy $<E_i>$. The vertical dashed lines at t_s - t_o = 230 s in Figure 7 mark the arrival of the interior Alfvén

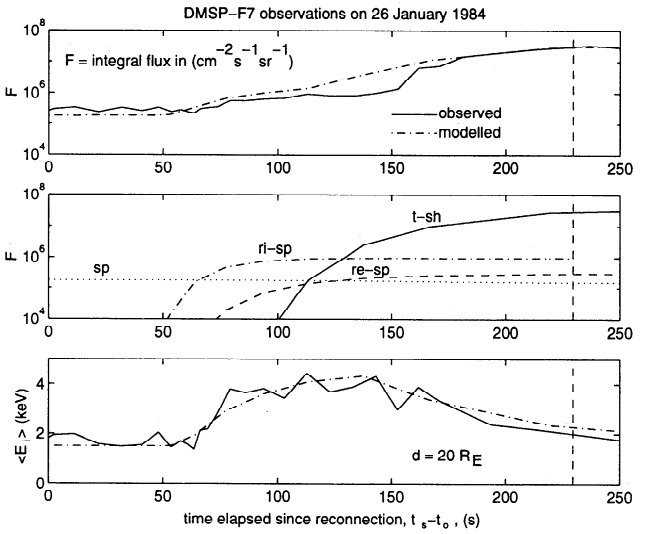

Figure 7. The evolution of integral number fluxes F and average ion energy $<E_i>$ as a function of time elapsed since reconnection (t_s - t_o), for an assumed distance from the satellite to the X line of $d = 20\ R_E$. (top) Total F, integrated over the energy range 30 eV to 30 keV, as observed on January 26, 1984 by the DMSP F7 satellite (solid line) and as modeled for the conditions given in Figure 2 (dot-dashed line). (middle) Contribution to the total modeled flux from the various populations (labeled as in Figure 2). (bottom) Average ion energies (both modeled and observed), computed from the energy of each channel weighted by its contribution to the total integral flux. Fluxes which fall below the one-count level are put equal to that level.

wave, assuming that the wave speed V_{Asp} is constant over the distance d. Since the ri-sp population is reflected off the interior wave, it is only seen prior to the arrival of the wave in this case. In reality, the interior wave will accelerate and overtake some of the ri-sp population it had previously generated by reflecting the sp ions. However, this also causes the kink at I to straighten as the field line evolves so that the current at the interior RD weakens. This is very likely to cause the reflection coefficient r_i to decrease with time elapsed since reconnection and to have become negligibly small by the time the wave reaches the satellite. We would then expect a more gradual decay in the flux of the ri-sp population than is shown in Figure 7.

Also as solid lines in the top and bottom panel of Figure 7 are the observed values of F and $<E_i>$. The time-elapsed since reconnection (t_s - t_o) at each observation time t_s is computed for the same assumed value for d of 20 R_E using the observed cutoff velocity $v_{ic} = d/(t_s - t_o)$. As the open/closed boundary is approached, no ion cutoff can be defined because fluxes at such high energies are below the one-count level. Thus we have extrapolated t_s - t_o down to zero using a polynomial fit as a function of t_s. This procedure correctly places the electron edge at t_s - t_o = 8 s (see following sections). The mean ion energy $<E_i>$ is computed from the energy of each channel, weighted by its contribution to the total integral flux. For both the observed and modeled $<E_i>$, fluxes which drop below the one-count level are put equal to that level. The data in Figure 4 reveal that one or two counts are often seen in the lowest-energy channels. The random

nature of these counts implies that some of this is noise, but there may also be a very low energy ionospheric population present. Neither such a low-energy population nor random noise was included in the simulated data and so low count rates (≤2) at low velocities (v < 300 km s^{-1}) were here excluded when calculating the observed $<E_i>$.

It can be seen that agreement between the modeled and observed fluxes and average energies is very good. This is significant because Figure 6, and thus the modelled values, were derived only from the distribution functions at the velocity cutoff, $f(v_{ic})$, whereas Figure 7 considers the whole of the spectra at each time. Figure 7 (top) shows that the total flux rises as the first (i.e., most energetic) ri-sp ions arrive after t_s - t_o = 50 s and then again as the t-sh ions begin to dominate at around t_s - t_o = 150 s. The former causes a rise in $<E_i>$ because the ri-sp population is energetic, the latter a fall because the t-sh population is of lower energy. Just before 150 s, the observed total F was increasingly lower than predicted until the t-sh population fluxes begin to dominate. This may be partially explained by the progressive straightening of the interior RD and the weakening of the interior current sheet. This is likely to cause the factor r_i to fall as the field line evolves away from the X line, an effect for which no allowance is made here. In addition, some progressive loss of the higher-energy sp ions may be a factor. However, the major differences in Figure 7 arise from the uncertainty in t_s - t_o for the observations. The rise in $<E_i>$ after t_s - t_o = 50 s is significant as it shows that the ion population seen between the electron edge (poleward of the open/closed separatrix) and the equatorward edge of the cusp cannot be regarded as a simple extension of the magnetospheric population to higher latitudes, as is also apparent from Figure 3.

As discussed above, either the decay of N_{sp} and/or the reflection coefficient r_i or the arrival of the interior wave (in the case of constant N_{sp}, r_i and V_{Asp}), will mean that the ri-sp population can no longer be seen. Thus, whereas at lower values of t_s - t_o the t-sh and ri-sp populations will dominate, at greater t_s - t_o the t-sh and re-sp populations will dominate. Thus we should expect the spectra in Figure 4 to migrate from the top to the bottom dotted line, as t_s - t_o increases. For the equatorward pass discussed here, this should occur with decreasing observation time t_s. Figures 4a-4c reveal exactly this behavior. The top dotted line is a generally good match to the spectra after 1246:07 UT, but before 1246:05 UT it is matched to the bottom dotted line. The transition is not smooth, indicating that the transition may have moved back and forth across the satellite, giving multiple partial crossings; nor is the change sudden, but, as discussed above, this may be caused by a decay in the reflection coefficient r_i and/or in the concentration of magnetospheric ions available for reflection N_{sp} as the interior wave propagates. Thus the satellite appears to have moved from the re-sp population to the ri-sp, as predicted. Furthermore, the first of the ri-sp population were seen at around 1246:06, when the best estimate of the lower cutoff velocity of the t-sh population is v_{ic} = 600 km s^{-1} (see Figure 4b) which is equal to the value of the local magnetospheric Alfvén speed V_{Asp} derived from Figure 6. This is also as predicted by Figure 7.

There are some interesting implications of the derived values for the interior wave Alfvén wave speed (V_{Asp} = 600 km s^{-1}) and the concentration of the magnetospheric sp population (N_{sp} = 4.3×10^5 m^{-3}). However, they are not central to the main point of this paper (which is the prediction, identification, and implications of the ri-sp population) and are discussed here only briefly in the appendix.

Implications

We have presented evidence that the ion populations seen by the DMSP F7 satellite on January 26, 1984 were caused by the interaction of the magnetosheath and magnetospheric plasmas with the two Alfvén waves which emanate from the magnetopause reconnection site. This equatorward pass was through a quasi-steady cusp, in that a clear cusp/mantle precipitation dispersion plume can be identified and the time elapsed since reconnection (t_s - t_o) decreases in a relatively smooth manner with observation time t_s. Note, however, that even for this apparently steady state case, the reconnection rate varies by a factor exceeding 2 [*Lockwood et al.*, 1994; *Lockwood and Davis*, 1996]. Because the reconnection rate is quasi-steady, conversion of the data from being displayed as a function of observation time (as in Figure 3) to its representation as a function of elapsed time since reconnection (as in the solid lines in Figure 7) is relatively straightforward. This transformation reveals the underlying structure in the data, predicted to exist as a function of elapsed time since reconnection t_s - t_o by the modelled dot-dash lines in Figure 7.

This underlying structure will always be present on newly opened field lines, but it will vary with the densities, temperatures, and Alfvén speeds on both sides of the magnetopause. In addition, the variation seen by a satellite (i.e., with observing time t_s) will often be complicated by boundary motions, reconnection rate variations, spatial structure, and a satellite path across curved convection streamlines. With these factors in mind, Figure 7 offers a physical interpretation of the various precipitation classifications reported on the dayside [*Newell and Meng*, 1992], as defined from prior studies [*Newell and Meng*, 1988; *Newell et al.*, 1991a; b]. The precipitation at t_s - t_o < 0 would be classed as central plasma sheet (CPS). Figure 3 shows that at the electron edge (inferred to be at 1246:20 UT), low fluxes of magnetosheath electrons arrive with energies up to about 700 eV, whereas magnetospheric electrons at energies greater than this are lost [see *Gosling et al.*, 1990b]. From the flight time of a 700-eV electron over the d = 20 R_E used in Figure 7, the electron edge is at about t_s - t_o = 8s. The ion flux continues almost unaltered (with only the loss of the very highest energies of the CPS population) onto open field lines, up to t_s - t_o ≈ 50 s., when the first ri-sp ions arrive. Precipitation classified as cusp by *Newell et al.* [1991a] was detected after 1246:09 (t_s = 129 s), when the cutoff velocity v_{ic} is 850 km s^{-1} (corresponding to an energy of 3.76 keV). For our assumed d of 20 R_E, the cusp boundary is at t_s - t_o of 150 s. The question arises as to how the precipitations at t_s - t_o in the interval 8-150 s would be classified. The schematic diagram by *Newell and Meng* [1992] shows that the precipitations in this region between CPS and cusp may be classed as either dayside boundary plasma sheet (BPS), void or LLBL. The modeled ion precipitation immediately equatorward of the cusp in Figure 7 has mean ion energy greater than the 3-keV threshold adopted by *Newell and Meng* [1988] to distinguish cusp and cleft. The fluxes of the t-sh ions just before t_s - t_o = 150 s are lower and the mean energy higher simply because the lower-energy ions have not yet had time to arrive

[*Lockwood and Smith*, 1993]. The presence of a mixture of magnetosheath-like and magnetosphere-like ion populations is also often used to define the LLBL. In this case, the sp population will have no ions with velocities above v_{ic} and the high-energy ions used to define the magnetospheric population would be the ri-sp. Thus we propose that the modeled mixture of t-sh and ri-sp populations, of the kind seen here at t_s - t_o from about 120 s to 150 s, would be classed as LLBL. Note that this precipitation is well into the open field line region: for a 1 km s^{-1} convection drift across the open/closed boundary, this precipitation would be found 120-150 km poleward of that boundary. Before t_s - t_o = 120s, the ri-sp population dominates, with negligible t-sh ions. This could be classed as either dayside BPS precipitation or void. We suggest that the times when the ri-sp population dominates would often be classed as BPS, particularly if some magnetospheric electron fluxes are maintained on open field lines [see *Daly and Fritz*, 1982; *Scholer et al.*, 1982; *Cowley and Lewis*, 1990]. The chances of both remnant magnetospheric electrons and the ri-sp population being seen simultaneously are higher if the ri-sp ions arrive at lower t_s - t_o because V_{Asp} is high. *Newell et al.* [1991b] consider the dayside BPS to be an extension of the nightside BPS; however, in the examples they present, the electron precipitation appears to evolve across the BPS from being like that within the CPS region to being like that in the LLBL. This evolution is consistent with newly opened field lines as electrons are lost. If the interior Alfvén wave has an even higher speed V_{Asp} it may arrive at the satellite before any detectable flux of the t-sh population, producing a gap between the ri-sp and t-sh dominant regions. That gap would be classed as void.

In addition, the arrival of the interior Alfvén wave will mark the onset of the change of the ionospheric convection in response to the curvature force on the newly opened field lines. Thus it will be the equatorward edge of the convection reversal boundary and of the region 1 field-aligned currents. Consequently, the situation shown in Figure 7 offers an explanation of the "circumpolar ion precipitation" (CPIP) classification of *Nishida et al.* [1993]. We identify the dayside CPIP with the ri-sp population, much of which would be on sunward convecting field lines (because it arrives before the Alfvén wave) and all of which is on open field lines (as identified by polar rain electron precipitation). Both of these features were found for the CPIP by Nishida et al. In general, the interior Alfvén wave accelerates so that it overtakes some of the ri-sp population it had previously generated. The wave then arrives in the center of the detectable ri-sp population and thus the convection reversal boundary would be in the center of the region of LLBL precipitation, as observed by *Newell et al.* [1991b].

It should be stressed that the accelerated ion population on the equatorward edge of the magnetosheath-like precipitations (usually classed as dayside BPS and here explained as magnetosphere ions reflected off the interior Alfvén wave) is an exceedingly common phenomenon [*Newell and Meng*, 1992]. In the majority of cases, the satellite will not follow an ionospheric streamline and then the BPS is then likely to show a sharp poleward boundary where time elapsed since reconnection (t_s - t_o) changes discontinuously. Examples like the pass discussed here (and others, for example that presented by *Pinnock et al.* [1993]) are valuable because the satellite orbit maintained a roughly constant orientation, with respect to the flow streamlines, such that t_s - t_o was a relatively smoothly varying function of the observation time t_s and the evolution of BPS precipitation into the LLBL and cusp precipitation classifications is clearly displayed.

Conclusions

The reconnection model of the dayside magnetosphere has been used to predict a variety of ion populations on open field lines. In the past, there have been a number of suggestions that magnetosphere-like ion populations may be extended onto open field lines, including time-of-flight effects and a magnetic bottle on open field lines due to the field minimum in the magnetic cusp field topology [*Daly and Fritz*, 1982; *Scholer et al.*, 1982; *Cowley and Lewis*, 1990]. The mechanism proposed here is much closer to that proposed by *Curran and Goertz* [1989], in that it invokes scattering off the current sheet. However, these authors studied chaotic particle orbits whereas we use here guiding-center particle motion with simple reflection and transmission coefficients at the current sheets, as adopted by *Cowley* [1982]. We have generalized the highly successful theory of Cowley to allow for reflection of the magnetospheric population off both the interior and exterior Alfvén waves which bound the reconnection layer.

The model is very successful in matching the ion precipitation data observed during the selected example of a cusp crossing by the DMSP F7 satellite on January, 26 1984. In particular, it predicts the observed accelerated ion population which is continuous with the cusp dispersion signature but of lower concentration. This population is not a simple extension of the magnetospheric population onto open field lines as fluxes at high energies are considerably greater than in the magnetosphere itself. Although we find strong evidence for acceleration, there is not clear evidence for the additional heating. This is because the unaccelerated magnetospheric population (sp) was not well resolved. The heating factors h_e and h_i were included here for generality; however, the data are equally well fitted with these factors reduced to unity and T_{sp} proportionally increased.

The model has the potential to predict the variety of precipitation classifications between CPS on closed field lines and the cusp/mantle plume on field lines which have been open for several minutes. These include LLBL, void, dayside BPS, and CPIP. Furthermore, it should be able to place these precipitation features relative to the convection reversal boundary and the region 1 field-aligned currents for a given set of conditions. Importantly, the LLBL, void, and dayside BPS classifications are all explained as being on open field lines. This is significant as the cusp/LLBL boundary has frequently been thought of as defining the open/closed separatrix because the BPS, void and LLBL classifications have been usually thought of as being on closed field lines.

Appendix: Implications of the Derived Speed of the Interior Alfvén Wave

In the main text, we use observations to estimate both the interior Alfvén speed (V_{Asp} = 600 km s^{-1}) and the concentration of field-aligned sp ions on closed field lines near the reconnection X line (N_{sp} = 4.3×10^5 m^{-3}). These place some constraints on the magnetospheric field B_{sp} in the vicinity of the X line. If the mean mass of the ion gas is a_i in atomic

mass units, the field required is given by:

$$B_{sp} = V_{Asp} (\mu_o N_{sp}^* a_i m_p)^{0.5} = \chi V_{Asp} (\mu_o N_{sp} m_p)^{0.5} \quad (A1)$$

where m_p is the proton mass and N_{sp}^* is the total concentration of the plasma from all sources, with all pitch angles. The factor χ is equal to $(a_i N_{sp}^*/N_{sp})^{0.5}$.

If we take $a_i = 1$ and $N_{sp}^* = N_{sp}$ (i.e. the sp population is protons, the only one present and isotropic), χ is unity and we require a B_{sp} of 17.6 nT. This is a low value, considering *Lockwood et al.* [1994] found that a value of 76 nT would be required at the nose of the magnetosphere to balance the observed solar wind dynamic pressure at this time. If the reconnection takes place away from the nose and nearer to a magnetic cusp (either in the near or the far hemisphere to the satellite), B_{sp} may indeed be lower than the 76 nT predicted for the nose of the magnetosphere. We can conclude that we need a factor χ which is about 76.0/17.6 = 4.3 (for a reconnection site at the nose of the magnetosphere) or less (for a reconnection site closer to a magnetic cusp where B_{sp} is lower). In section A1, we consider factors which could increase χ and thus help to resolve this apparent anomaly. In section A2 we look at the implications of the major factor in χ, namely, the loss cone distribution of the magnetospheric sp population.

A1. Factors Which Can Increase χ

The DMSP F7 ion detector only observes ions close to zero pitch angle; thus all inferred distribution functions are field-parallel slices through the full three-dimensional distribution functions. As a result, the derived concentration N_{sp} will be lower than the three-dimensional total N_{sp}^* if there is an anisotropy of the ion gas. In particular, the DMSP F7 satellite in the topside ionosphere detects only those sp ions in the loss cone and so will considerably underestimate the concentration of the population in the magnetosphere if it has a loss cone (or a double loss cone) distribution. To give the $\chi = 4.3$ discussed above, the anisotropy must cause the ratio N_{sp}^*/N_{sp}) to be 18.5.

Furthermore, the detector does not resolve the mass of the ions and the presence of species such as He^{2+}, He^+, and O^+ will cause a_i to exceed unity. There may be a cold ionospheric component present equatorward of the cusp which causes the few observed counts at low velocities. Including these counts as a real ionospheric population gives N_{sp}^*/N_{sp}) $\approx$ 2, which increases χ by a factor of only 1.4. However, such ions should appear as a sharp peak at $2V_{Asp}$ = 1200 km s^{-1} in the ri-sp population [*Cowley*, 1982], which is not seen in Figure 6. This appears to eliminate the possibility of any larger increase in χ due to a denser ionospheric population. It may be that the detected sp population is not pure protons; however, even a very large O^+ component of 5% only raises a_i up to 1.75 and the factor χ by 1.3.

We also suggest here an interesting additional possibility. The ions of the modelled t-sh and re-sp populations which arrive at the satellite at $t_s - t_o < 230$ s are super-Alfvénic (see Figure 7). For the inferred V_{Asp}, the ions observed by DMSP F7 after 1246:06 were super-Alfvénic in the vicinity of the X line (see Figure 4). Such ions are injected across or reflected at (for the t-sh and the re-sp populations, respectively), the exterior RD and can subsequently catch and pass through the interior RD. Thus they must be included in the total N_{sp}^*; they will therefore act to slow the interior Alfvén wave. The more the wave is slowed, the more of the t-sh and re-sp populations will be able to catch it, further slowing it. Thus the magnetosheath densities may then effectively be able to control V_{Asp}, as well as V_{Ash}. The interior wave originates from the X line diffusion region, and one possibility is that the initial additional density is introduced from the magnetosheath by the diffusion process.

A2. Effects of the Loss Cone Distribution of the sp Population

However, the major factor increasing χ (and thus solving the anomaly) is likely to be the anisotropy of the magnetospheric population. This is because the sp population seen at low altitudes is inside the loss cone, and thus N_{sp} is much lower than N_{sp}^* at the magnetopause (fluxes are larger at larger pitch angles, outside the loss cone). On reflection at the magnetopause Alfvén waves, scattering causes the loss cone to be filled and it is seen in neither the ri-sp nor the re-sp populations. Thus the reflection coefficients r_i and r_e given in the text are overestimates as they are derived from the fluxes of field-parallel ions only. Values derived from full three-dimensional distribution functions would be lower. Substituting the field parallel value, N_{sp}, with the value of $N_{sp}^* = 18.5 N_{sp}$, as inferred above for a subsolar reconnection site, the reflection coefficients r_i and r_e are reduced to just 0.005 and 0.02, respectively.

This anisotropy factor is also relevant to the assumption, used in the main text to derive Figure 7, that the fluxes of source populations at the magnetopause do not initially change with elapsed time since reconnection and, in particular, that the flux of sp ions does not progressively decay. In reality, the sp ions are lost, either by transmission into the magnetosheath or by reflection (that is, they become part of the ri-sp or re-sp populations). The field-aligned sp ions are lost above a velocity threshold which decays with increasing elapsed time since reconnection, $t_s - t_o$. However, this loss will initially not be reflected in the highest energies of the field-aligned parts of the ri-sp and re-sp populations; this is because quasi-trapped ions from larger pitch angles are scattered into the field-aligned direction on reflection. The ri-sp and re-sp populations seen at low altitudes will thus decay more slowly, with the longer time constant of the loss of quasi-trapped magnetosphere ions at larger pitch angles. This effect can be neglected in Figure 7 because on the timescales for significant loss, the integral flux and average energy become dominated by the precipitating magnetosheath flux.

Acknowledgments. M.L. is supported by the United Kingdom Particle Physics and Astronomy Research Council. The authors thank M.P. Freeman of BAS for valuable discussions of this work and C.J. Davis of RAL for the spectral fitting software employed.

The Editor thanks M.F. Smith and A.S. Rodger for their assistance in evaluating this paper.

References

Alem, F., and D.C. Delcourt, Nonadiabatic precipitation of ions at the cusp equatorward edge, *J. Geophys. Res., 100*, 19,321, 1995.

Burch, J. L., Quasi-neutrality in the polar cusp, *Geophys. Res. Lett., 12*, 469-472, 1985.

Cowley, S. W. H., The causes of convection in the Earth's magnetosphere: A review of developments during IMS, *Rev. Geophys., 20*, 531, 1982.

Cowley, S.W.H., Theoretical perspectives on the magnetopause: A tutorial review, in *Physics of the Magnetopause, Geophys. Monogr. Ser.*, vol. 90, edited by P. Song, B.U.Ö. Sonnerup and M.F. Thomsen, AGU, Washinton, D.C., p. 29, 1995.

Cowley, S.W.H, and C.J. Owen, A simple illustrative model of open flux tube motion over the dayside magnetopause, *Planet. Space Sci., 37*, 1461, 1989.

Cowley, S.W.H., and Z.V. Lewis, Magnetic trapping of energetic particles on open dayside boundary layer flux tubes, *Planet. Space Sci., 38*, 1343, 1990.

Cowley, S.W.H., D.J. Southwood, and M.A. Saunders, Interpretation of magnetic field perturbations in the Earth's magnetopause boundary, *Planet. Space Sci., 31*, 1237, 1983.

Curran, D.B., and C.K. Goertz, Particle distributions in a two-dimensional reconnection field geometry, *J. Geophys. Res., 94*, 272, 1989.

Daly, P.W., and T.A. Fritz, Trapped electron distributions on open field lines, *J. Geophys. Res., 87*, 6081, 1982.

de Hoffmann, F., and E. Teller, Magneto-hydrodynamic shocks, *Phys. Rev., 80*, 692, 1950.

Fuselier, S.A., D.M. Klumpar, and E.G. Shelley, Ion reflection and transmission during reconnection at the Earth's subsolar magnetopause, *Geophys. Res. Lett., 18*, 139, 1991.

Gosling, J.T., M.F. Thomsen, S.J. Bame, R.C. Elphic, and C.T. Russell, Cold ion beams in the low-latitude boundary layer during accelerated flow events, *Geophys. Res. Lett., 17*, 2245, 1990a.

Gosling, J.T., M.F. Thomsen, S.J. Bame, T.G. Onsanger, and C.T. Russell, The electron edge of the low-latitude boundary layer during accelerated flow events, *Geophys. Res. Lett., 17*, 1833, 1990b.

Hapgood, M.A., and D.A. Bryant, Exploring the magnetospheric boundary layer, *Planet. Space Sci., 40*, 1431, 1992.

Heyn, M.F., H.K. Biernat, R.P. Rijnbeek, and V.S. Semenov, The structure of reconnection layers, *J. Plasma Phys., 40*, 235, 1988.

Hudson, P.D., Discontinuities in an isotropic plasma and their identification in the solar wind, *Planet. Space Sci., 18*, 1611, 1970.

Levy, R.H., H.E. Petschek, and G.L. Siscoe, Aerodynamic aspects of magnetosheath flow, *AIAA J., 2*, 2065, 1964.

Lin, Y., and L.C. Lee, Structure of the dayside reconnection layer in resistive MHD and hybrid models, *J. Geophys. Res., 98*, 3919, 1993.

Lin, Y., and L.C. Lee, Reconnection layer at the flank magnetopause in the presence of shear flow, *Geophys. Res. Lett., 21*, 855, 1994.

Lockwood, M., The location and characteristics of the reconnection X line deduced from low-altitude satellite and ground-based observations: 1. Theory, *J. Geophys. Res., 100*, 21791, 1995.

Lockwood, M., and C.J. Davis, An analysis of the accuracy of magnetopause reconnection rate variations deduced from cusp ion dispersion characteristics, *Ann. Geophys., 14*, 149, 1996.

Lockwood, M., and M.F. Smith, The variation of reconnection rate at the dayside magnetopause and cusp ion precipitation, *J. Geophys. Res., 97*, 14,841, 1992.

Lockwood, M., and M.F. Smith, Comment on "Mapping the dayside ionosphere to the magnetosphere according to particle precipitation characteristics" by Newell and Meng, *Geophys. Res. Lett., 20*, 1739, 1993.

Lockwood, M., and M.F. Smith, Low- and mid-altitude cusp particle signatures for general magnetopause reconnection rate variations: I - Theory, *J. Geophys. Res., 99*, 8531, 1994.

Lockwood, M., T.G. Onsager, C.J. Davis, M.F. Smith, and W.F Denig, The characteristics of the magnetopause reconnection X line deduced from low-altitude satellite observations of cusp ions, *Geophys. Res. Lett., 21*, 2757, 1994.

Lockwood, M., C.J. Davis, M.F. Smith, T.G. Onsager, and W.F Denig, The location and characteristics of the reconnection X line deduced from low-altitude satellite and ground-based observations: 2. DMSP and EISCAT radar data, *J. Geophys. Res., 100*, 21,803, 1995.

Newell, P.T., and C.-I. Meng, The cusp and the cleft/LLBL: Low altitude identification and statistical local time variation, *J. Geophys. Res., 93*, 14,549, 1988.

Newell, P.T. and C.-I. Meng, Mapping the dayside ionosphere to the magnetosphere according to particle precipitation characteristics, *Geophys. Res. Lett., 19*, 609, 1992.

Newell, P.T., W.J. Burke, C.-I. Meng, E.R. Sanchez, and M.E. Greenspan, Identification and observation of the plasma mantle at low altitude, *J. Geophys. Res., 96*, 35, 1991a.

Newell, P.T., W.J. Burke, E.R. Sanchez, C.-I. Meng, M.E. Greenspan, and C.R. Clauer, The low-latitude boundary and the boundary plasma sheet at low altitude: Prenoon precipitation regions and convection reversal boundaries, *J. Geophys. Res., 96*, 21,013, 1991b.

Nishida, A., T. Mukai, H. Hayakawa, A. Matsuoka, and K. Tsuruda, Unexpected features of the ion precipitation in the so-called cleft/low-latitude boundary layer region: Association with sunward convection and occurrence on open field lines, *J. Geophys. Res., 98*, 11,161, 1993.

Onsager T.G., C.A. Kletzing, J.B. Austin, and H. MacKiernan, Model of magnetosheath plasma in the magnetosphere: Cusp and mantle particles at low-altitudes, *Geophys. Res. Lett., 20*, 479, 1993.

Petschek, H.E., Magnetic field annihilation, in *AAS-NASA Symposium of Physics of Solar Flares*, edited by W. N. Hess, *NASA Spec. Publ., SP-50*, 425, 1964.

Phan, T.-D., G. Paschmann, W. Baumjohann, N. Sckopke, and H. Lühr, The magnetosheath region adjacent to the dayside magnetopause: AMPTE-IRM observations, *J. Geophys. Res., 99*, 121, 1994.

Pinnock, M., A.S. Rodger, J.R. Dudeney, K.B. Baker, P.T. Newell, R.A. Greenwald, and M.E. Greenspan, Observations of an enhanced convection channel in the cusp ionosphere, *J. Geophys. Res., 98*, 3767, 1993.

Scholer, M., P.W. Daly, G. Paschmann, and T.A. Fritz, Field line topology determined by energetic particles during a possible magnetopause reconnection event, *J. Geophys. Res., 87*, 6073, 1982.

Smith, M.F., and Rodgers, D.J., Ion distributions at the dayside magnetopause, *J. Geophys. Res., 95*, 11617, 1991.

S.W.H. Cowley, Department of Physics and Astronomy, Leicester University, Leicester, LE1 7RH, England, United Kingdom. (e-mail:swhcl@ion.le.ac.uk)

M. Lockwood, Rutherford Appleton Laboratory, Chilton, Didcot, Oxfordshire, OX11 0QX, England, United Kingdom. (e-mail:m.lockwood@rl.ac.uk)

T.G. Onsager, Space Environment Center, National Oceanic and Atmospheric Administration, Boulder CO, 80303-3328. (e-mail: tonsager@sel.noaa.gov)

(Received April 4, 1996; revised June 3, 1996;
accepted June 19, 1996.)